Indium-decorated Pd Nanocubes Degrade Nitrate Anions Rapidly

Welman C. Elias,[a,b,¥] *Kimberly N. Heck,*[b,¥] *Sujin Guo,*[c,d,f] *Sadegh Yazdi,*[e,†] *Ciceron Ayala,*[b] *S. Sophia Grossweiler,*[b] *Josiel B. Domingos,*[a] *Emilie Ringe*[e,‡,§] *and Michael S. Wong*[b,c,d,e,f]*

[a]Universidade Federal de Santa Catarina, Campus Trindade, Florianópolis - SC, 88040-900, Brazil; [b]Department of Chemical and Biomolecular Engineering, [c]Department of Civil and Environmental Engineering, [d]Nanosystems Engineering Research Center for Nanotechnology-Enabled Water Treatment, [e]Department of Materials Science and NanoEngineering, [f]Department of Chemistry, Rice University, Houston, TX, 6100 S. Main Street, Houston, Texas 77005.

Keywords: In-on-Pd nanocubes; bimetallic catalyst, nitrate reduction; structure sensitivity

Abstract: Indium-decorated palladium nanoparticles (In-on-PdNPs) are active for room-temperature catalytic reduction of aqueous nitrate, where the active sites are metallic In atoms on the Pd surface. The PdNPs are pseudo-spherical in shape, and it is unclear if their faceted nature plays a role in nitrate reduction. We synthesized different-sized, cube-shaped NPs with differing In coverages (sc%), and studied the resultant In-on-Pd-nanocubes (NCs) for nitrate reduction. The NCs exhibited volcano-shape activity dependence on In sc%, with peak activity around 65-75 sc%. When rate constants were normalized to undercoordinated atoms (at edge+corners), the NCs exhibited near-identical maximum activity (20×-higher than In-on-PdNPs) at $\rho_{In/Pd\ edge+corner}$ ~0.5 (~5 In atoms per 10 edge and corner atoms). NCs with a higher In edge+corner density ($\rho_{In/Pd\ edge+corner}$ ~1.5) were less active but did not generate NH_4^+ at nitrate conversions tested up to 36%. Edge-decorated cubes may be the structural basis of improved bimetallic catalytic denitrification of water.

[¥]*These authors contributed equally to the manuscript.*
[†]*Current address: Renewable and Sustainable Energy Institute, University of Colorado-Boulder, 4001 Discovery Dr., Denver, Colorado 80309-0027*
[‡]*Department of Materials Science and Metallurgy, University of Cambridge, 27 Charles Babbage Road, Cambridge CB3 0FS, UK*
[§]*Department of Earth Sciences, University of Cambridge, Downing Street, Cambridge CB2 3EQ, UK*
Corresponding author: mswong@rice.edu

1. Introduction

Drinking water contaminated with the nitrogen oxyanions, NO_3^- and NO_2^-, can cause serious human health problems including cancer, hypertension, and methemoglobinemia (blue baby syndrome). [1-6] From a broader environmental prospective, the excess of nitrogen oxyanions in water bodies can cause algal bloom dead zones fatal for aquatic life.[7-9] Bimetallic PdIn catalysts are active for the water-phase reduction of nitrate selectively to non-toxic dinitrogen gas over ammonium (Scheme 1),[10-12] and are a promising approach for the treatment of nitrate contaminated waters compared to ion exchange and reverse osmosis systems[13]. The latter are effective in treating nitrate contamination, but they generate secondary waste streams. Nitrate has been shown to be reducible to nitrite by bimetallic InPd sites, with the nitrite further reduced to dinitrogen or ammonium on monometallic Pd sites (Scheme 1).[14-16] We recently studied In-decorated Pd nanoparticle (In-on-Pd NPs) catalysts using x-ray absorption spectroscopy (XAS), activity measurements and density functional theory (DFT) calculations. [17, 18] *In situ* XAS experiments showed that In metal oxidized in the presence of nitrate and the oxidized In reduced in the presence of H_2-containing water, indicating the role of In atoms act as a redox site for the nitrate-to-nitrite reduction step. DFT calculations suggested that this rate-limiting step occurs with the lowest activation barrier over In ensembles of 4 to 6 atoms (close to the observed maximum nitrate reduction activity at ~40% surface coverage (sc)).[17]

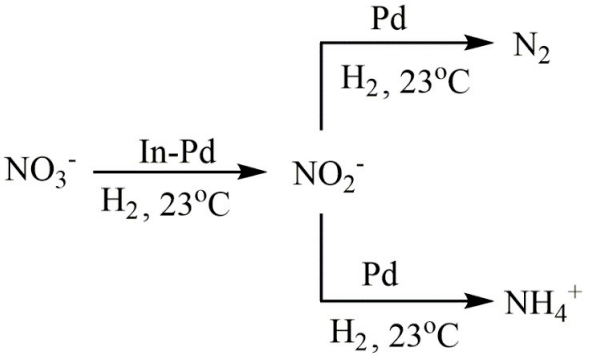

Scheme 1. Nitrate reduction reaction.

These NPs (as well as those in supported metal catalysts) were sphere-shaped, which led us to consider the effect of shape on nitrate reduction bimetallic catalysis. In general, NP size and shape affect catalytic activity and selectivity due to differences in the relative number of terrace

vs. edge atoms of an exposed crystal plane of the metal surface,[19-22] as corroborated by metal site characterization studies like CO chemisorption.[23] Werth and coworkers showed that monometallic Pd NPs with well-defined shapes were active for nitrite reduction, and that shapes that exposed Pd (100) planes had higher activity.[24] The activity differences among the different facets disappeared at high nitrite concentrations, indicating the particle shape effect on catalysis was observable only when reactant coverage was low.

The distribution of the two metals that compose bimetallic NPs (*e.g.*, core@shell, complete alloy, and Janus structures) directly affects catalytic properties.[25-27] Xia and coworkers studied the selective decomposition of hydrazine to H_2 over differently shaped Pd NPs modified with surface Ir to form core@shell structures. While better activity was found over all the Ir-modified NPs, the shape of the Ir@Pd NPs also affected the reaction, with cubes being more selective to H_2 over ammonia compared to octahedral and cuboctahedral NPs. The authors proposed that the higher H_2 selectivity from the Ir@Pd nanocubes arises from the better efficiency of Ir(100) faces in facilitating heteroatom splitting of NH_2 surface species and recombination of N- and H-adatoms to form N_2 and H_2 relative to Ir(111) faces predominant in the octahedral and cuboctahedral NPs.[28]

The shape dependence for nitrate reduction catalysis over bimetallic InPd catalysts has not yet been studied. To assess the importance of Pd NP shape in this study, we synthesized and characterized three series of cube-shaped Pd NPs of a given cube size with a range of In surface coverages. We compared the nitrate reduction activity of these In-on-Pd NCs against that of the quasi-spherical NPs. We analyzed the rate constants with respect to In-sc and NC edge and corner atoms. With these insights, we propose In atoms on the edges and corners of the Pd NCs as active sites for nitrate reduction, based on observed changes in dinitrogen/ammonium selectivity with In-sc.

Experimental

2.1 Synthesis of Palladium Nanoparticles

Pd NCs were synthesized by a procedure reported previously (Scheme A1).[29] Briefly, in a two-neck round flask, 105 mg of PVP, 60 mg of ascorbic acid (AA) and 300 to 900 mg of KBr were dissolved in 8 mL of water and heated for 10 minutes at 80 °C under magnetic stirring. 57 mg of Na_2PdCl_4 in 3 mL of water was then added, and the solution heated for 4 hours at 80 °C.

The solution turned black, confirming the reduction of the Pd precursor salt. Acetone (3x 35 mL) was then added to the sols to aid in precipitating the nanoparticles, and to remove excess of PVP, which was then centrifuged at 500 RPM for 40 min to collect the Pd NCs. The standard, pseudo-spherical NPs (termed here as nanospheres or "NSs") were synthesized using the same procedure except omitting the KBr. Pd content of the washed precipitates was quantified by performing inductively coupled plasma optical emission spectrometry (ICP-OES, Perkin Elmer Optima 8300) of a solution of 10 µL of the as-synthesized Pd NPs dissolved in 200 µL aqua regia diluted in 9790 µL water (for a final volume of 10 mL). After accounting for the nanocube/nanosphere particle size, the Pd particle concentrations of the as-synthesized suspensions can be calculated (Table A1 of Appendix A)

2.2 Synthesis of Indium-on-Palladium Nanoparticles

The In-sc used in the Pd nanospheres was calculated based on magic cluster models for a cuboctahedron, where the amount of In atoms needed to fill the 6^{th}, shell around a magic cluster of 5 closed shells of Pd atoms (which approximates the 3 nm PdNS) (Table A2). For the nanocubes, the In sc% was calculated modeling it as a perfect cube, composed by a central atom surrounded by shells that form the cube shape, where the amount of In atoms needed to fill the 29^{th}, 47^{th}, and 59^{th} shell around a cluster of 28, 46 and 58 shells of Pd atoms (which approximates the 11, 18 and 23 nm PdNCs, respectively).

The various In surface coverage percentage (In sc%) for the four different Pd NPs were obtained by mixing different amounts of $InCl_3 \cdot 4H_2O$ solution (0.04 M) with 2 mL of the Pd NPs, previously quantified by ICP (Tables A3-A5 and A7). The solution was bubbled with hydrogen gas for 30 min at a flow rate of ~200 mL min^{-1} under stirring (Scheme A2), to reduce the In precursor salt.[17] There was no subsequent washing step prior to catalyst testing; it was thus assumed all In salt precursor was retained in the In-on-Pd catalysts (Table A8).

For comparison, a supported catalyst was also prepared with a Pd:In weight ratio of 93:7 (equivalent to the weight ratio of the In-on-PdNC11 of 65 sc%) through wet impregnation.[17] Briefly, 622 mg of a commercially available 1 wt% Pd on Al_2O_3 ("Pd/Al_2O_3") catalyst was weighed and 102 µL of 11.9 mg mL^{-1} of indium chloride solution tetrahydrate was added to a final aqueous volume of 30 mL. The resulting material was reduced under H_2 gas for 30 min.

2.3 Nanoparticle Characterization

Transmission electron microscopy (TEM) images were obtained using a JEOL 2010 transmission electron microscope operating at an accelerating voltage of 120 kV. The particle size distribution was calculated by counting at least 200 particles using ImageJ. pH measurements were taken using a VWR sympHony SB20 meter with a standard pH electrode.

The STEM-HAADF high resolution and composition images were obtained using a FEI Titan Themis^3 S/TEM equipped with image and probe spherical aberration correctors.

2.4 Catalytic Activity Studies

Batch nitrate reduction experiments were conducted in a screw-cap bottle (125 mL, Alltech) with PTFE-sealed threads and a PTFE-silicone septum.[30] The catalytic assays were carried out at room temperature in aqueous media, adding In-on-PdNPs amount such the total In concentration per reaction was 0.5 mg-In L^{-1} in a total volume of 50 mL (Table A8). Experiments of monometallic catalysts were also conducted for Pd NPs, $InCl_3 \cdot 4H_2O$ precursor salt, In_2O_3, a physical mixture of In_2O_3 + Pd NPs, and 1 wt% Pd/Al_2O_3 (metal concentration of 0.5 mg L-1 of Pd or In). These experiments were meant to show the importance of In salt being reduced onto Pd NPs. The solution was then bubbled simultaneously with hydrogen gas (100 mL min^{-1}, reductant) and carbon dioxide gas (100 mL min^{-1}, pH buffer of 4-6) for 30 min. 50 µL of a $NaNO_3$ solution (10 mg-NO_3^- mL^{-1}) was then injected into the sealed bottle to start the reaction, such that the initial NO_3^- concentration was 10 mg-NO_3 L^{-1} (2.3 mg-N L^{-1}). Aliquots of 1 mL were withdrawn periodically from the reactor (Scheme A3) to quantify NO_3^-, NO_2^-, and ammonium. The In-on-Pd NPs showed negligible UV-vis absorbance, so no separation of the particles from the reaction medium was performed. Griess test was used to analyze nitrite concentration. Ammonium was analyzed using Nessler's reagent. Nitrate measurements were made using a nitrate ion selective electrode (Cole-Parmer, lower detection limit 0.1 ppm).[31]

The observed reaction rate constant k_{obs} was calculated by a first-pseudo order (H_2 gas was in excess) dependence on nitrate concentration (eqn 1.):

$$-\frac{dC_{NO_3^-}}{dt} = k_{obs} C_{NO_3^-}$$

where C_{NO3}^- is the nitrate concentration and t is reaction time. The surface metal, face metal and edge+corner metal normalized reaction rates constants k_{cat}, k_{cat}'and k_{cat}'', were calculated from k_{obs} and are showed in eqn 2 to 4:

$$k_{cat} = \frac{k_{obs}}{C_{surf}} \quad \text{eqn 2}$$

$$k_{cat}' = \frac{k_{obs}}{C_{face}} \quad \text{eqn 3}$$

$$k_{cat}'' = \frac{k_{obs}}{C_{e+d}} \quad \text{eqn 4}$$

were C_{surf}, C_{face} and C_{e+d} is the total concentration of In and Pd on the surface, on the face (excluding edge and corner atoms) and on the edges and corners of the catalyst in the reaction medium, respectively.

The C_{surf}, C_{face} and C_{e+d}, were obtained using the magic cluster model, in which the model consists of a single atom surrounded by 12 atoms in the first shell, for a *fcc* cuboctahedra NPs, assuming and a perfect cuboctahedron with eight faces (111) and six faces (100) (see Table A2, A6, and A8 for more details). The NC structure were obtained applying a cube model, where a *fcc* cube with six perfect faces (100) were modeled.

2.5 Calculations of nanoparticle surface atoms

We calculated the amount of In atoms associated only with Pd edge and corner atoms, using a probability equation, that assumes the Pd NCs as perfect cubes and In atoms deposition can occurs on Pd edge atoms as also in In deposited edge atoms, depending on the In sc% (eqn 5):

$$\rho_{\frac{¿}{Pd}edge+corner} = \frac{(¿\, sc\,\%\, x\, edge\,\%)}{N_{edge}\, N_{atom}} \quad \text{eqn 5}$$

where In edge+corner density $\rho_{In/Pd\ edge+corner}$ is the number of In atoms on the edge per Pd edge atom, "In sc%" is the In percentage of surface coverage, "edge %" is the percentage of atoms that are edge atoms in the Pd particle, N_{edge} is the number of edges that compose the cube (12 edges)

or the cuboctahedron (24 edges) NPs, and N_{atom} is the number of atoms that compose the 1-D edges and corners of the NPs, calculated using the mean edge length of the Pd NCs (Table A2).

2.6 Coordination number calculation

The coordination number for the edge and corner atoms were calculated using eqn 6.

$$CN = \frac{\left(N_{ac}\, x\, CN_{ac}\right) + \left(N_{ae}\, x\, CN_{ae}\right)}{N_{edge+corner}}$$

where CN is the coordination number, N_{ac} is number of atoms on the corner of a perfect cube (N_{ac} = 8 atoms) or a perfect cuboctahedron (N_{ac} = 12 atoms), CN_{ac} is the CN of the corner atoms (Scheme A4), N_{ae} is the number of atoms in the edges, not considering the corners (Table A2 and A6), CN_{ae} is the CN of edge atoms, not considering the corners (Scheme A4) and $N_{edge+corners}$ is the total number of atoms in the edges and corners of the NPs (Table A2 and A6).

2.7 Determination of dinitrogen selectivity

As established by previous studies, N_2 is the major product of the nitrate reduction reaction catalyzed by InPd catalysts,[15, 32] and intermediates such as the NO and N_2O only form in trace amounts [15, 33-35]. Only ammonia and nitrite were considered in the selectivity determination of N_2 (S_{N2}), as given in eqn 7

$$S_{N2} = 100\% - S_{NH4+} - S_{NO2-} \qquad \text{eqn 7}$$

where S_{NH4+} and S_{NO2} are the selectivity to ammonium and nitrite, respectively. S_{NH4+} and S_{NO2} can be calculated from eqn. 8 and 9:

$$S_{NH_4^+} = ¿¿ \qquad \text{eqn 8}$$

$$S_{NO_2^-} = ¿¿ \qquad \text{eqn 9}$$

where $[NO_3^-]_0$ is the initial concentration of the nitrate and $[NO_3^-]$ is the concentration of nitrate after time *t* of reaction. The concentration of $[NO_2^-]$ and $[NH_4^+]$ in the reaction of NO_3^- reduction were determined by the calibration curves shown in Fig. A1 and A2.

3 Results and Discussion

3.1 Synthesis and Characterization of NPs

We used bright-field transmission electron microscopy (TEM) to determine the size, shape and polydispersity of the Pd NPs, and confirmed the spheres were 3.0 ± 0.6 nm, and cubes had edge lengths of 11.2 ± 1.8 nm, 18 ± 3 nm and 23 ± 2 nm (error reflects one standard deviation obtained from over 200 NPs; Fig. 1a-h). These NPs are hereafter labeled as PdNS3, PdNC11, PdNC18 and PdNC23, respectively. Two perpendicular edges of each cube were measured and plotted versus each other to confirm cubic morphology (Fig. 1i-l). The monometallic Pd NSs and NCs were used as cores for the synthesis of bimetallic In-on-Pd NPs with different calculated In sc% (Scheme A5).

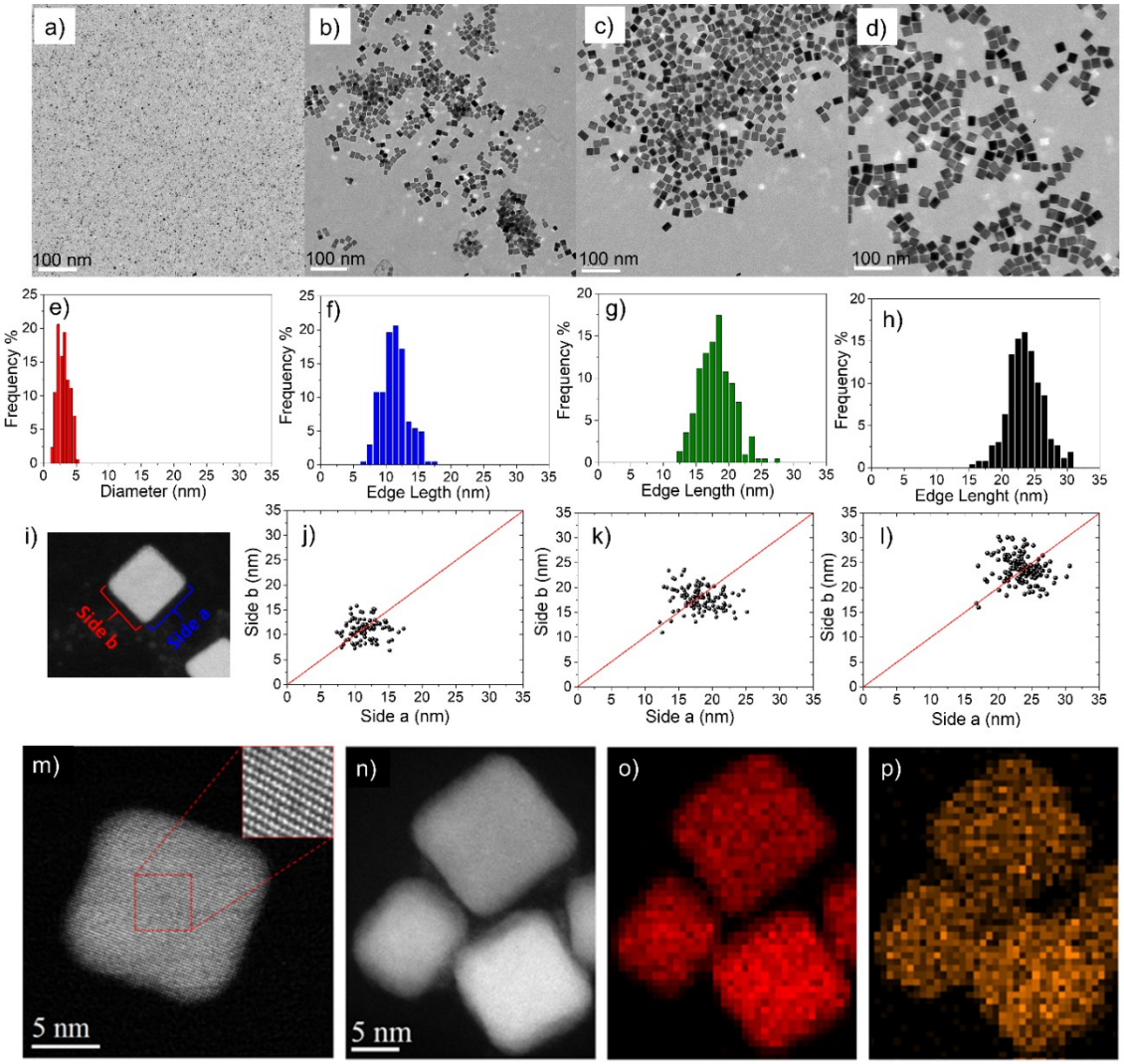

Figure 1. Characterization of PdNPs. TEM micrographs of (a) PdNS3. (b) PdNC11. (c) PdNC18 and (d) PdNC23. Scale bar = 100 nm. Average edge length distribution histograms for (e) PdNS3, (f) PdNC11, (g) PdNC18, (h) and PdNC23 respectively. Each bar represents the total number of NPs of a particle diameter ± 0.25 nm for the PdNS3 and ± 0.50 nm for PdNC11. PdNC18. and PdNC23. (i) model of Pd NCs edge lengths measurements, plot of side a versus side b for the (j) PdNC11, (k) PdNC18, and (l) PdNC23. respectively. The red line is for a perfect cube (a = b). HAADF-STEM characterization of (m) PdNC11 and (n) In-on-PdNC11 (65 sc%) after nitrate reduction reaction. Energy dispersive X-ray spectroscopy (EDS) composition maps of (o) Pd-L and (p) In-L edge for In-on-PdNC11 (65 sc%) after nitrate reduction reaction.

Fig. 1m shows a HAADF-STEM image of the 65 sc% In-on-PdNC11. The contrast in HAADF-STEM images is proportional to $Z^{1.8}$, where Z is the atomic number. Fig. 1a shows clear terminated edges for the Pd cube before In coating, while a darker shell surrounds the Pd cube

after In coating (Fig. 1n). Although In atoms are heavier than Pd and the In shell is expected to be brighter than the Pd core in HAADF-STEM images, the shell is darker because In did not cover the Pd cube surface. The dark shell consists of single atoms of In that form a thin non-uniform layer on the Pd surface, consistent with the expected In decorated Pd NPs structure of In-on-Pd.[36, 37] Single atoms, identified as In, were imaged by HAADF-STEM close to Pd cubes after In coating (Fig. A3 and A4). Based on the average 25% drop of contrast from the Pd core to the In shell in HAADF-STEM images and on the assumption that contribution of other possible elements such as K, Br, Cl, C, O and N present in the synthesis (Fig. A5) is negligible, the surface coverage of Pd cube by In atoms is estimated to be 80%, which is somewhat close to the 65% estimated by our calculations (Entry 3 in Table A3). EDS composition map (Fig. 1o and p) also confirms the Pd core/In decorated structure of the 65 sc% In-on-PdNC11. No change in the cube structure was observed in HAADF-STEM images before and after reaction (Fig. A3 and A4).

3.2 Activity of In-on-Pd NPs

Having verified the structure of the In-on-Pd NPs, we then quantified the activity of the In-on-Pd NP catalysts for nitrate reduction. Pseudo-first order rate constants, k_{obs}, were determined from NO_3^- concentration-time profiles (Fig. A6 and A7). Since both In and Pd have active roles in the reaction,[3, 4, 15, 38] k_{obs} was normalized to the number of In and Pd atoms on the surface to obtain the surface-atom normalized pseudo-first order rate constant, k_{cat} (L $g_{surface\ metal}^{-1}$ min^{-1}, Table A8). As shown in Fig. 2a, the k_{cat} rate constants for all catalysts initially increase with the addition of In on the surface of Pd NPs. Further increasing the In sc% causes the rate constant to decrease, with all catalysts demonstrating a characteristic volcano-shaped dependence of activity on In loading. In our earlier study on In-on-Pd nanoparticle catalysis [17], we concluded that the volcano dependence on In sc% was attributable to the presence of surface In ensembles of varying nitrate oxygen abstraction activity. A bimetallic electronic effect was responsible for the most active ensembles (containing 4 to 6 In atoms), which were the most prevalent at the volcano peak.[17] Control experiments using monometallic Pd NPs, $InCl_3 \cdot 4H_2O$ precursor salt, In_2O_3, a physical mixture of In_2O_3 + Pd NPs, and 1 wt% Pd/Al_2O_3 did not show catalytic activity for the reaction, indicating the In-on Pd bimetallic structure was necessary.

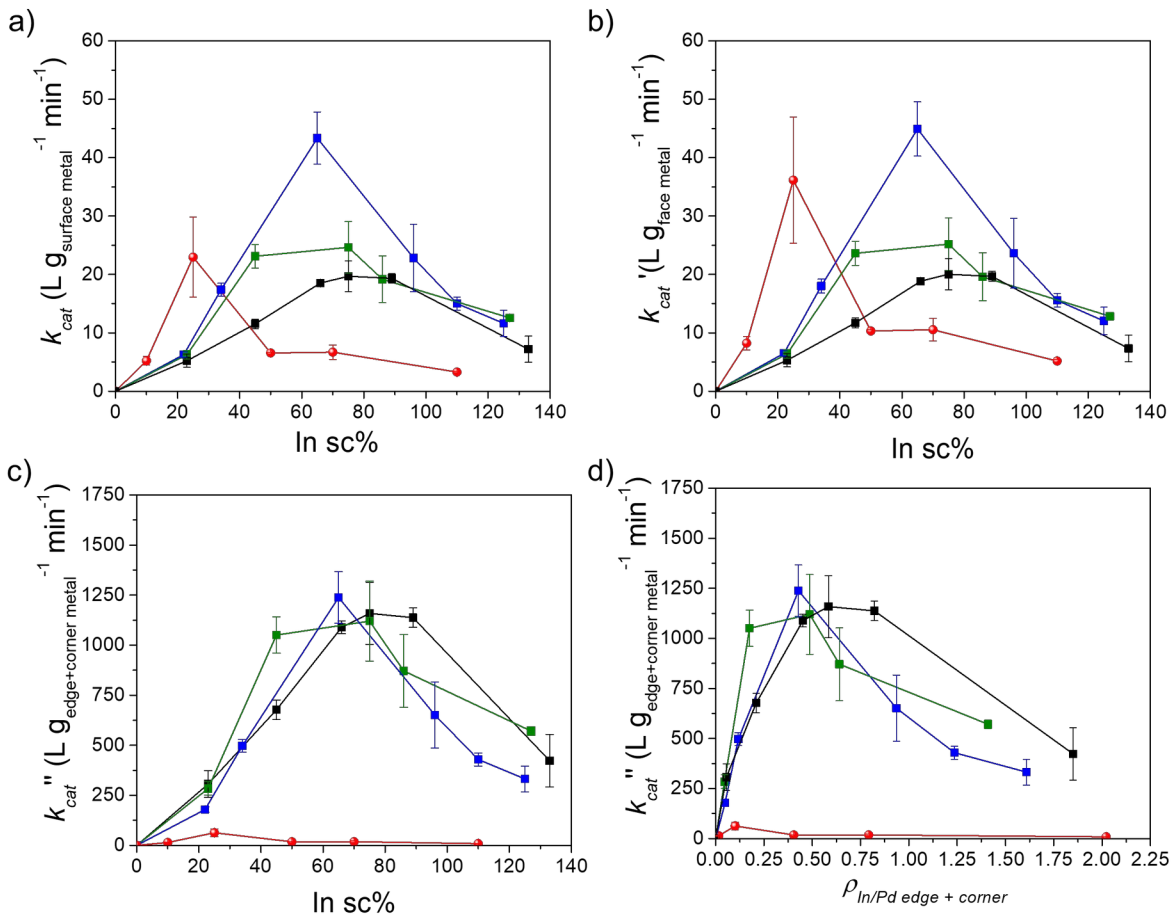

Figure 2. Nitrate reduction reaction kinetic data for In-onPdNS3 (●), In-on-PdNC11 (■), In-on-PdNC18 (■), and In-on-PdNC23 (■). Catalytic rate constants normalized by (a) the total surface atoms of the NPs (k_{cat}), (b) face atoms of the NPs (k_{cat}'), and (c) edge+corner atoms of the NPs (k_{cat}'') plotted against In calculated surface coverage. (d) k_{cat}'' values from panel (c) plotted against the In coverage of Pd edge+corner atoms of the Pd particle ($\rho_{In/Pd\ edge+corners}$).

While the maximum rate constant for In-on-PdNS3 occurs at a similar sc% as our previous work [17] (25 sc% vs 40 sc%), it is a much higher value (23.0 vs 7.6 L $g_{surface\_metal}^{-1}$ min^{-1}). We attribute this to the improved synthesis method, which incorporated a number of wash and centrifuge steps, which likely removed more of the PVP polymer stabilizing agent from the sol. There is evidence that PVP can lower catalytic activity of suspended NPs [39-41].

If all surface atoms were equally active, one would expect the per-surface-atom activity to be the same from one type of NP to the other, provided they had similar surface compositions (same In sc%). Instead, the observed activity per surface atom varied widely between the differently sized NCs and the NSs. The maximum k_{cat} found for each type of morphology

differed, with values of 23.0 ± 6.9, 43.3 ± 4.5, 24.6 ± 4.4, and 19.7 ± 2.6 L $g_{surface\_metal}^{-1}$ min^{-1} found for In-on-PdNC11, In-on-PdNC18, In-on-PdNC23, and In-on-PdNS3 respectively. The surface coverage at which the maximum activity was observed differed, with the maximum occurring at 65, 75, and 75 sc% for the 11, 18, and 23 nm NCs, and at 25 sc% for the spheres. For comparison, the In-on-Pd/Al_2O_3 (which had an equivalent Pd:In weight ratio as that of the most active In-onPdNC11, 65 sc%) showed 1.5-fold lower activity. This can likely be attributed in part to the deposition of In on the Al_2O_3 surface instead of Pd.[17]

Intrigued by the differences in the catalytic activity peaks observed for the different sizes of In-on-Pd NPs, we calculated rate constants by re-normalizing k_{obs} to the different types of surface atoms: the face or terrace atoms (excluding the edge and corner atoms) k_{cat}' (L $g_{face\ metal}^{-1}$ min^{-1}), and the edge and corner atoms k_{cat}'' (L $g_{edge+corner\ metal}^{-1}$ min^{-1}). Edge and corner atoms are expected to be more catalytic active, because they have lower coordination numbers (*CN*) (Table 1), tending to bind adsorbates more strongly, which in turn weakens intramolecular bonds of the transition state species [42-45]. While there was expectedly little difference in the volcano curves after re-normalization to terrace atoms (Fig. 2b), the volcano curves aligned much more closely after re-normalization to edge and corner atoms (Fig. 2c). They also became much larger in value compared to that of the spherical particles. The 3-nm In-on-Pd NS sample had lower activity than the NCs after modeling the NS shape as a cuboctahedron and normalizing by edge and corner atoms (Scheme A5). This suggests that the InPd catalyst is more effective when In atoms are localized on the edge/corners of the cube than on the edge/corners of the sphere shape.

Table 1. Coordination numbers (CNs) of edge and corner atoms and normalized rate constants for the most active In-on-Pd catalysts.

Catalyst	**Average CN of edge and corner atom**	**Average CN of terrace atom**	**k_{cat}'' (L $g_{edge+corner\ metal}^{-1}$ min^{-1})**
25 sc% In-on-PdNS3	6.8	8.3	63 ± 19
65 sc% In-on-PdNC11	5.0	8.0	1238 ± 128
75 sc% In-on-PdNC18	5.0	8.0	1120 ± 199
75 sc% In-on-PdNC23	5.0	8.0	1159 ± 155

We next plotted k_{cat}" to the theoretical number of In atoms per Pd edge and corner atom ($\rho_{In/Pd\ edge+corner}$) (Fig. 2d). Arguably, the k_{cat}"-$\rho_{In/Pd\ edge+corner}$ curves show better overlap than the k_{cat}"-In sc% curves, suggesting the active sites are better associated with In atoms on the edge/corners of the NCs than with the NC faces. The peaks of the activity curves are more coincident around 0.3-0.7 $In/Pd_{edge/corner\text{-}atoms}$ than around 40-100 In sc%.

3.3 Selectivity to Ammonium and Nitrite

In general, over all the catalysts, the selectivity to nitrite increased and then decreased as a function of nitrate conversion (Fig. 3). Nitrite selectivities decreased at higher nitrate conversions due to nitrite undergoing further reduction to form ammonia and N_2. For materials with a low $\rho_{In/Pd\text{-}edge}$, ammonium selectivities exceeded nitrite selectivities at the highest nitrate conversions, presumably due to insufficient amount of N-containing surface species needed for the N-N coupling to occur for eventual N_2 formation. Interestingly, materials with a high $\rho_{In/Pd\text{-}edge}$ did not form ammonia.

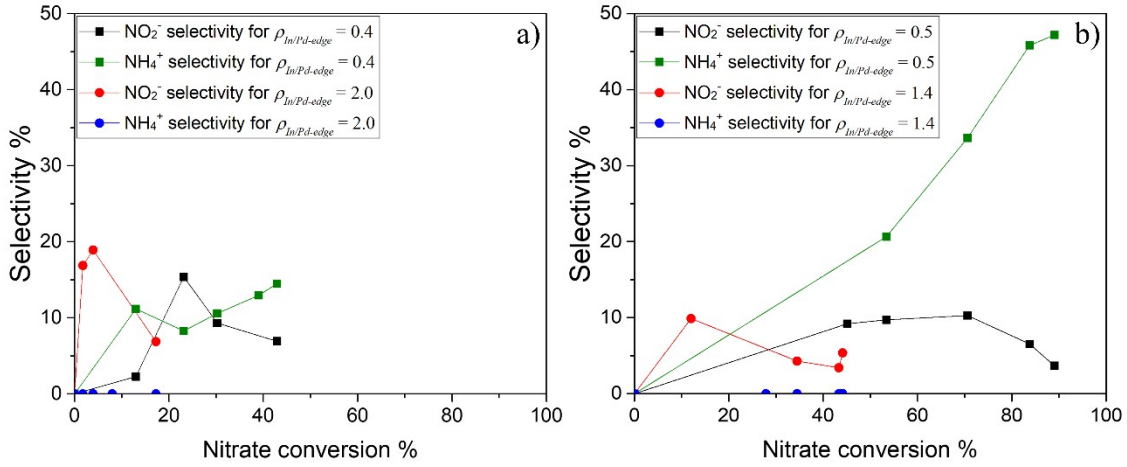

Figure 3. Typical nitrite and ammonium selectivity-conversion data: (a) In-onPdNS3 with low and high In edge+corner density $\rho_{In/Pd\text{-}edge}$ (0.4 and 2.0), and (b) In-onPdNC18 with low and high $\rho_{In/Pd\text{-}edge}$ (0.5 and 1.4).

We analyzed nitrite and ammonia formation more closely at three nitrate conversion values (10, 20, 36%) for the three NC sizes, at high and low In edge+corner density values (Fig. 4). For low $\rho_{In/Pd\ edge+corner}$ (~0.5, Fig. 4a), the concentration of NO_2^- increased with increasing nitrate conversion. At the higher edge density (~1.5, Fig. 4c), nitrite concentrations were generally higher and did not increase as much with conversion. Ammonium concentrations

increased with nitrate conversion for catalysts with low $\rho_{In/Pd\ edge+corner}$ (Fig. 4b), and ammonia was definitely not detected at the high $\rho_{In/Pd\ edge+corner}$ (Fig. 4d).

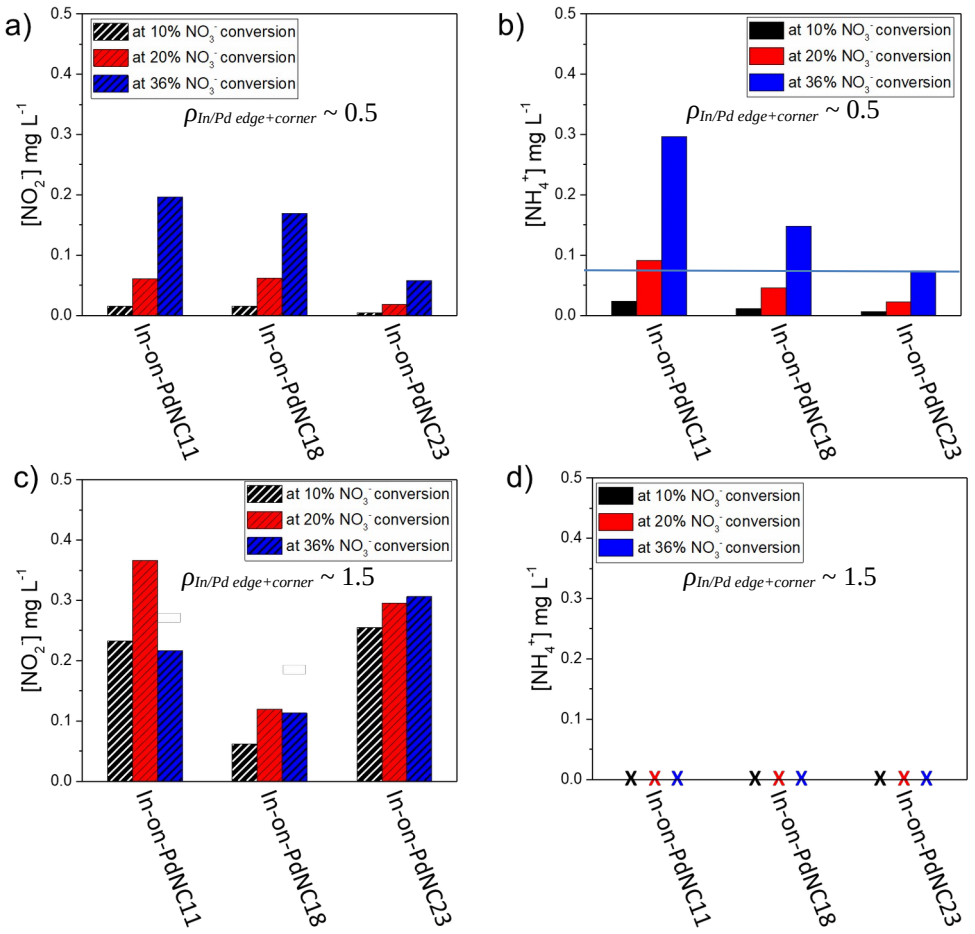

Figure 4. Nitrite and ammonium concentration plotted against the In-on-PdNCs for different NO_3^- conversions: (a) $[NO_2^-]$ and (b) $[NH_4^+]$ for In-on-PdNC's with $\rho_{In/Pd\ edge+corner}$ ~ 0.5; (c) $[NO_2^-]$ and (d) $[NH_4^+]$ for In-onPdNC's with $\rho_{In/Pd\ edge+corner}$ ~ 1.5.

The generally accepted surface mechanism for nitrate reduction by InPd catalysts involves two different active sites. The rate-limiting step is catalyzed by the In ensembles, which absorb and reduce NO_3^- to NO_2^-. The role of the Pd sites is two-fold, wherein they both reduce NO_2^- to form N_2 or NH_4^+, as well as generate hydrogen adatoms to reduce oxidized In.[18] We suggest a similar mechanism exists for the NCs, except that the majority of transformations occur on the cube edges and corners, as implicated by our structure-activity investigations. For

the NCs with low In density (e.g., $\rho_{In/Pd\ edge+corner}$ ~ 0.5, Scheme 2a), the first step is the NO_3^- reduction by In sites to form NO_2^- (Fig. 4a), followed by the migration of the NO_2^- to a Pd site or desorption from the In site to the solvent. If additional surface N-species are present at adjacent Pd sites, then dinitrogen is formed. However, if the NO_2^- is isolated from other formed N-species, formation of ammonium is favored. This can be seen in the large amount of NH_4^+ generated over NCs with relatively smaller $\rho_{In/Pd\ edge+corner}$ (Fig. 4b), which increases as a function of nitrate conversion.

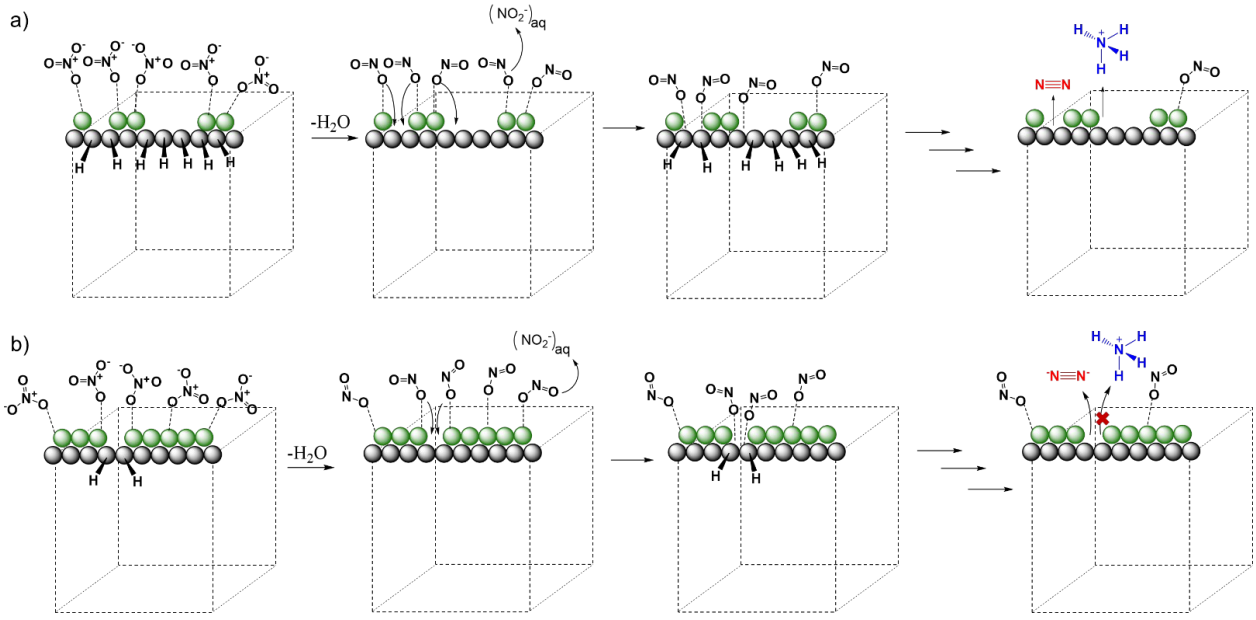

Scheme 2. Proposed mechanism for NO_3^- catalyzed by In-on-Pd nanocubes on the edges and corners for: (a) low $\rho_{In/Pd\ edge+corner}$ (~0.5) and (b) high $\rho_{In/Pd\ edge+corner}$ (~1.5).

We observed that NCs generated no ammonia formation at a higher $\rho_{In/Pd\ edge+corner}$ at nitrate conversions up to 36% (Fig. 4d). We hypothesize that the larger In domains block more of the exposed Pd sites at high In densities (e.g. $\rho_{In/Pd\ edge+corner}$ ~1.5, Scheme 2b). This serves to funnel the formed NO_2^- (Fig. 4c) onto fewer available Pd sites, making N-species encounters on the Pd sites more likely leading to dinitrogen. The proposed mechanism is consistent with prevailing model of bimetal catalyzed nitrate reduction catalysis, where rate-limiting step occurs with the lowest activation barrier over In ensembles of 4 to 6 atoms, [17] similar to the peak activity observed for the In-on-Pd NCs ($\rho_{In/Pd\ edge+corner}$ ~ 0.5). The selectivity trend agrees with published observations, though a structural explanation for low/zero ammonia selectivity at high In content

remains limited. Barbosa and coworkers observed a similar decrease in ammonia selectivity with In content in PdIn catalysts prepared by successive impregnation.[46] Miró and coworkers observed similar selectivity results for Pd-In catalysts supported on Al_2O_3, where decreasing the Pd:In ratio from 1.0:0.25 to 1.0:1.2 decreased the ammonium selectivity from ~1 to ~0 mg L^{-1} N-NH_4^+ (at ~40% NO_3^- conversion). The authors suggested this effect was due to relative metal distributions, as XPS analysis showed the catalysts had relatively Pd-rich cores and In-rich shells.[47]

4. Conclusion

We report the successful synthesis of four shaped In-on-Pd NP catalysts (3 nm NSs and 11, 18, and 23 nm NCs), characterized them by electron microscopy, and determined their activity for the reduction of aqueous nitrate. HAADF-STEM results indicated that In deposits on the surface of the Pd NCs forming a metal-on-metal structure. Convergence of the volcano curves for the different-sized NC catalysts after normalizing the rate constants to edge and corner cube atoms and plotted against In edge+corner density $\rho_{In/Pd\ edge+corner}$ strongly suggests that the nitrate reduction reaction proceeded preferentially on the edge and corner atoms of NCs. While less active, NCs with a higher In edge+corner density ($\rho_{In/Pd\ edge+corner}$ ~1.5) did not produce ammonium at nitrate conversions tested up to 36%, which we attribute to higher likelihood of N-coupling reactions on the Pd edges. The identification of the most active sites has the prospect of improving catalyst design not only for catalytic denitrification reactions, but potentially for other oxyanions as well.

Appendix A. Supplementary data

The following are Supplementary data to this article:

Declaration of Competing Interest

There are no conflicts to declare.

Corresponding Author

mswong@rice.edu

Acknowledgements

We would like to thank Dr. A. Stender and Dr. S. Kasiraju for helpful discussions. W.E. and J.D. acknowledge CNPq and CAPES for financial support received under the Science Without Borders Program (SWE 207700/2014-1). E.R and S.Y. acknowledge support from the ACS-PRF Grant #56256-DNI5. We acknowledge partial support by the NSF Nanosystems Engineering Research Center for Nanotechnology-Enabled Water Treatment (ERC-1449500).

REFERENCES

[1] B. Hansen, L. Thorling, J. Schullehner, M. Termansen, T. Dalgaard, Groundwater nitrate response to sustainable nitrogen management, Sci Rep, 7 (2017) 8566. DOI: 10.1038/s41598-017-07147-2.

[2] K. Wick, C. Heumesser, E. Schmid, Groundwater nitrate contamination: factors and indicators, J Environ Manage, 111 (2012) 178-186. DOI: 10.1016/j.jenvman.2012.06.030.

[3] R. Zhang, D. Shuai, K.A. Guy, J.R. Shapley, T.J. Strathmann, C.J. Werth, Elucidation of Nitrate Reduction Mechanisms on a Pd-In Bimetallic Catalyst using Isotope Labeled Nitrogen Species, ChemCatChem, 5 (2013) 313-321. DOI: 10.1002/cctc.201200457.

[4] J. Martínez, A. Ortiz, I. Ortiz, State-of-the-art and perspectives of the catalytic and electrocatalytic reduction of aqueous nitrates, Applied Catalysis B: Environmental, 207 (2017) 42-59. DOI: 10.1016/j.apcatb.2017.02.016.

[5] S. Jung, S. Bae, W. Lee, Development of Pd-Cu/hematite catalyst for selective nitrate reduction, Environ Sci Technol, 48 (2014) 9651-9658. DOI: 10.1021/es502263p.

[6] T. Ye, D.P. Durkin, N.A. Banek, M.J. Wagner, D. Shuai, Graphitic Carbon Nitride Supported Ultrafine Pd and Pd-Cu Catalysts: Enhanced Reactivity, Selectivity, and Longevity for Nitrite and Nitrate Hydrogenation, ACS Appl Mater Interfaces, 9 (2017) 27421-27426. DOI: 10.1021/acsami.7b09192.

[7] H.W. Paerl, W.S. Gardner, M.J. McCarthy, B.L. Peierls, S.W. Wilhelm, Algal blooms: noteworthy nitrogen, Science, 346 (2014) 175. DOI: 10.1126/science.346.6206.175-a.

[8] X. Chen, L. Yang, L. Xiao, A. Miao, B. Xi, Nitrogen removal by denitrification during cyanobacterial bloom in Lake Taihu, Journal of Freshwater Ecology, 27 (2012) 243-258. DOI: 10.1080/02705060.2011.644405.

[9] A.P. Murphy, Chemical removal of nitrate from water, Nature, 350 (1991) 223-225. DOI: 10.1038/350223a0.

[10] K.A. Guy, H. Xu, J.C. Yang, C.J. Werth, J.R. Shapley, Catalytic Nitrate and Nitrite Reduction with Pd−Cu/PVP Colloids in Water: Composition, Structure, and Reactivity

Correlations, The Journal of Physical Chemistry C, 113 (2009) 8177-8185. DOI: 10.1021/jp810049y.

[11] J. Jung, S. Bae, W. Lee, Nitrate reduction by maghemite supported Cu-Pd bimetallic catalyst, Applied Catalysis B: Environmental, 127 (2012) 148-158. DOI: 10.1016/j.apcatb.2012.08.017.

[12] F.M. Zoppas, F.A. Marchesini, A. Devard, A.M. Bernardes, E.E. Miró, Controlled deposition of Pd and In on carbon fibers by sequential electroless plating for the catalytic reduction of nitrate in water, Catalysis Communications, 78 (2016) 59-63. DOI: 10.1016/j.catcom.2016.02.012.

[13] K.N. Heck, S. Garcia-Segura, P. Westerhoff, M.S. Wong, Catalytic Converters for Water Treatment, Acc Chem Res, 52 (2019) 906-915. DOI: 10.1021/acs.accounts.8b00642.

[14] F. Epron, F. Gauthard, C. Pinéda, J. Barbier, Catalytic Reduction of Nitrate and Nitrite on Pt–Cu/Al2O3 Catalysts in Aqueous Solution: Role of the Interaction between Copper and Platinum in the Reaction, Journal of Catalysis, 198 (2001) 309-318. DOI: 10.1006/jcat.2000.3138.

[15] U. Prüsse, M. Hähnlein, J. Daum, K.-D. Vorlop, Improving the catalytic nitrate reduction, Catal Today, 55 (2000) 79-90. DOI: 10.1016/S0920-5861(99)00228-X.

[16] Z. Gao, Y. Zhang, D. Li, C.J. Werth, Y. Zhang, X. Zhou, Highly active Pd-In/mesoporous alumina catalyst for nitrate reduction, J Hazard Mater, 286 (2015) 425-431. DOI: 10.1016/j.jhazmat.2015.01.005.

[17] S. Guo, K. Heck, S. Kasiraju, H. Qian, Z. Zhao, L.C. Grabow, J.T. Miller, M.S. Wong, Insights into Nitrate Reduction over Indium-Decorated Palladium Nanoparticle Catalysts, ACS Catalysis, 8 (2017) 503-515. DOI: 10.1021/acscatal.7b01371.

[18] Y.B. Yin, S. Guo, K.N. Heck, C.A. Clark, C.L. Coonrod, M.S. Wong, Treating Water by Degrading Oxyanions Using Metallic Nanostructures, ACS Sustainable Chemistry & Engineering, 6 (2018) 11160-11175. DOI: 10.1021/acssuschemeng.8b02070.

[19] W.T. Ralston, G. Melaet, T. Saephan, G.A. Somorjai, Evidence of Structure Sensitivity in the Fischer-Tropsch Reaction on Model Cobalt Nanoparticles by Time-Resolved Chemical Transient Kinetics, Angew Chem Int Ed Engl, 56 (2017) 7415-7419. DOI: 10.1002/anie.201701186.

[20] R. van den Berg, G. Prieto, G. Korpershoek, L.I. van der Wal, A.J. van Bunningen, S. Laegsgaard-Jorgensen, P.E. de Jongh, K.P. de Jong, Structure sensitivity of Cu and CuZn catalysts relevant to industrial methanol synthesis, Nat Commun, 7 (2016) 13057. DOI: 10.1038/ncomms13057.

[21] G. Collins, M. Schmidt, C. O'Dwyer, J.D. Holmes, G.P. McGlacken, The origin of shape sensitivity in palladium-catalyzed Suzuki-Miyaura cross coupling reactions, Angew Chem Int Ed Engl, 53 (2014) 4142-4145. DOI: 10.1002/anie.201400483.

[22] H. Zhang, M. Jin, Y. Xiong, B. Lim, Y. Xia, Shape-Controlled Synthesis of Pd Nanocrystals and Their Catalytic Applications, Accounts of Chemical Research, 46 (2012) 1783-1794. DOI: 10.1021/ar300209w.

[23] M.J. Lundwall, S.M. McClure, D.W. Goodman, Probing Terrace and Step Sites on Pt Nanoparticles Using CO and Ethylene, The Journal of Physical Chemistry C, 114 (2010) 7904-7912. DOI: 10.1021/jp9119292.

[24] D. Shuai, D.C. McCalman, J.K. Choe, J.R. Shapley, W.F. Schneider, C.J. Werth, Structure Sensitivity Study of Waterborne Contaminant Hydrogenation Using Shape- and Size-Controlled Pd Nanoparticles, ACS Catalysis, 3 (2013) 453-463. DOI: 10.1021/cs300616d.

[25] S. Alayoglu, B. Eichhorn, Rh-Pt bimetallic catalysts: synthesis, characterization, and catalysis of core-shell, alloy, and monometallic nanoparticles, J Am Chem Soc, 130 (2008) 17479-17486. DOI: 10.1021/ja8061425.

[26] C. Langlois, Z.W. Wang, D. Pearmain, C. Ricolleau, Z.Y. Li, HAADF-STEM imaging of CuAg core-shell nanoparticles, Journal of Physics: Conference Series, 241 (2010) 012043. DOI: 10.1088/1742-6596/241/1/012043.

[27] M. Hosseini, T. Barakat, R. Cousin, A. Aboukaïs, B.L. Su, G. De Weireld, S. Siffert, Catalytic performance of core–shell and alloy Pd–Au nanoparticles for total oxidation of VOC: The effect of metal deposition, Applied Catalysis B: Environmental, 111-112 (2012) 218-224. DOI: 10.1016/j.apcatb.2011.10.002.

[28] X. Xia, L. Figueroa-Cosme, J. Tao, H.C. Peng, G. Niu, Y. Zhu, Y. Xia, Facile synthesis of iridium nanocrystals with well-controlled facets using seed-mediated growth, J Am Chem Soc, 136 (2014) 10878-10881. DOI: 10.1021/ja505716v.

[29] W.C. Elias, A.M. Signori, L. Zaramello, B.L. Albuquerque, D.C. de Oliveira, J.B. Domingos, Mechanism of a Suzuki-Type Homocoupling Reaction Catalyzed by Palladium Nanocubes, ACS Catalysis, 7 (2017) 1462-1469. DOI: 10.1021/acscatal.6b03490.

[30] Y.-L. Fang, K.N. Heck, P.J.J. Alvarez, M.S. Wong, Kinetics Analysis of Palladium/Gold Nanoparticles as Colloidal Hydrodechlorination Catalysts, ACS Catalysis, 1 (2011) 128-138. DOI: 10.1021/cs100067k.

[31] H. Qian, Z. Zhao, J.C. Velazquez, L.A. Pretzer, K.N. Heck, M.S. Wong, Supporting palladium metal on gold nanoparticles improves its catalysis for nitrite reduction, Nanoscale, 6 (2014) 358-364. DOI: 10.1039/c3nr04540d.

[32] U. Prüsse, K.-D. Vorlop, Supported bimetallic palladium catalysts for water-phase nitrate reduction, Journal of Molecular Catalysis A: Chemical, 173 (2001) 313-328. DOI: 10.1016/S1381-1169(01)00156-X.

[33] B.P. Chaplin, J.R. Shapley, C.J. Werth, The Selectivity and Sustainability of a Pd–In/γ-Al2O3 Catalyst in a Packed-Bed Reactor: The Effect of Solution Composition, Catalysis Letters, 130 (2009) 56-62. DOI: 10.1007/s10562-009-9883-4.

[34] S. Hamid, M.A. Kumar, W. Lee, Highly reactive and selective Sn-Pd bimetallic catalyst supported by nanocrystalline ZSM-5 for aqueous nitrate reduction, Applied Catalysis B: Environmental, 187 (2016) 37-46. DOI: 10.1016/j.apcatb.2016.01.035.

[35] S. Hamid, M.A. Kumar, J.-I. Han, H. Kim, W. Lee, Nitrate reduction on the surface of bimetallic catalysts supported by nano-crystalline beta-zeolite (NBeta), Green Chemistry, 19 (2017) 853-866. DOI: 10.1039/c6gc02349e.

[36] C. Zhang, J. Sha, H. Fei, M. Liu, S. Yazdi, J. Zhang, Q. Zhong, X. Zou, N. Zhao, H. Yu, Z. Jiang, E. Ringe, B.I. Yakobson, J. Dong, D. Chen, J.M. Tour, Single-Atomic Ruthenium Catalytic Sites on Nitrogen-Doped Graphene for Oxygen Reduction Reaction in Acidic Medium, ACS Nano, 11 (2017) 6930-6941. DOI: 10.1021/acsnano.7b02148.

[37] H. Wei, K. Huang, D. Wang, R. Zhang, B. Ge, J. Ma, B. Wen, S. Zhang, Q. Li, M. Lei, C. Zhang, J. Irawan, L.-M. Liu, H. Wu, Iced photochemical reduction to synthesize atomically dispersed metals by suppressing nanocrystal growth, Nature Communications, 8 (2017). DOI: 10.1038/s41467-017-01521-4.

[38] N. Barrabés, J. Sá, Catalytic nitrate removal from water, past, present and future perspectives, Applied Catalysis B: Environmental, 104 (2011) 1-5. DOI: 10.1016/j.apcatb.2011.03.011.

[39] W.C. Elias, R. Eising, T.R. Silva, B.L. Albuquerque, E. Martendal, L. Meier, J.B. Domingos, Screening the Formation of Silver Nanoparticles Using a New Reaction Kinetics Multivariate Analysis and Assessing Their Catalytic Activity in the Reduction of Nitroaromatic Compounds, The Journal of Physical Chemistry C, 118 (2014) 12962-12971. DOI: 10.1021/jp503280y.

[40] S. Campisi, M. Schiavoni, C. Chan-Thaw, A. Villa, Untangling the Role of the Capping Agent in Nanocatalysis: Recent Advances and Perspectives, Catalysts, 6 (2016) 185. DOI: 10.3390/catal6120185.

[41] Y. Zhao, J.A. Baeza, N. Koteswara Rao, L. Calvo, M.A. Gilarranz, Y.D. Li, L. Lefferts, Unsupported PVA- and PVP-stabilized Pd nanoparticles as catalyst for nitrite hydrogenation in aqueous phase, Journal of Catalysis, 318 (2014) 162-169. DOI: 10.1016/j.jcat.2014.07.011.

[42] A.P. Umpierre, E. de Jesús, J. Dupont, Turnover Numbers and Soluble Metal Nanoparticles, ChemCatChem, 3 (2011) 1413-1418. DOI:10.1002/cctc.201100159.

[43] B.E. Hayden, Particle Size and Support Effects in Electrocatalysis, Accounts of Chemical Research, 46 (2013) 1858-1866. DOI: 10.1021/ar400001n.

[44] S.S. Tafreshi, A. Roldan, N.H. de Leeuw, Density Functional Theory Study of the Adsorption of Hydrazine on the Perfect and Defective Copper (100), (110), and (111) Surfaces, The Journal of Physical Chemistry C, 118 (2014) 26103-26114. DOI: 10.1021/jp5078664.

[45] B. Ni, X. Wang, Face the Edges: Catalytic Active Sites of Nanomaterials, Advanced Science, 2 (2015) 1500085. DOI: 10.1002/advs.201500085.

[46] D.P. Barbosa, P. Tchiéta, M.d.C. Rangel, F. Epron, The use of a cation exchange resin for palladium–tin and palladium–indium catalysts for nitrate removal in water, Journal of Molecular Catalysis A: Chemical, 366 (2013) 294-302. DOI: 10.1016/j.molcata.2012.10.008.

[47] F.A. Marchesini, S. Irusta, C. Querini, E. Miró, Spectroscopic and catalytic characterization of Pd–In and Pt–In supported on Al2O3 and SiO2, active catalysts for nitrate hydrogenation, Applied Catalysis A: General, 348 (2008) 60-70. DOI:10.1016/j.apcata.2008.06.026.